American Mineralogist, Volume 92, pages 1031–1037, 2007

Investigation of synthetic $Mg_{1.3}V_{1.7}O_4$ spinel with MgO inclusions: Case study of a spinel with an apparently occupied interstitial site

Hinako Uchida,[1,*] Kevin Righter,[2] Barbara Lavina,[3,4] Matthew M. Nowell,[5] Stuart I. Wright,[5] Robert T. Downs,[1] and Hexiong Yang[1]

[1]Department of Geosciences, University of Arizona, Tucson, Arizona 85721-0077, U.S.A.
[2]Mailcode KT, NASA Johnson Space Center, 2101 NASA Parkway, Houston, Texas 77058, U.S.A.
[3]High Pressure Science and Engineering Center, University of Nevada Las Vegas, Las Vegas, Nevada 89154-4002, U.S.A.
[4]GSECARS, University of Chicago, 5734 S. Ellis Avenue, Chicago, Illinois 60637, U.S.A.
[5]EDAX-TSL, Draper, Utah 84020, U.S.A.

Abstract

A magnesium vanadate spinel crystal, ideally MgV_2O_4, synthesized at 1 bar, 1200 °C and equilibrated under FMQ + 1.3 log f_{O_2} condition, was investigated using single-crystal X-ray diffraction, electron microprobe, and electron backscatter diffraction (EBSD). The initial X-ray structure refinements gave tetrahedral and octahedral site occupancies of $^{T}(Mg_{0.966}\square_{0.034})$ and $^{M}(V^{3+}_{0.711}V^{4+}_{0.109}Mg_{0.180})$, respectively, along with the presence of 0.053 apfu Mg at an interstitial octahedral site (16*c*). Back-scattered electron (BSE) images and electron microprobe analyses revealed the existence of an Mg-rich phase in the spinel matrix, which was too small (≤3 μm) for an accurate chemical determination. The EBSD analysis combined with X-ray energy dispersive spectroscopy (XEDS) suggested that the Mg-rich inclusions are periclase oriented coherently with the spinel matrix. The final structure refinements were optimized by subtracting the X-ray intensity contributions (~9%) of periclase reflections, which eliminated the interstitial Mg, yielding a structural formula for spinel $^{T}Mg^{M}(V^{3+}_{1.368}V^{4+}_{0.316}Mg_{0.316})O_4$. This study provides insight into possible origins of refined interstitial cations reported in the literature for spinel, and points to the difficulty of using only X-ray diffraction data to distinguish a spinel with interstitial cations from one with coherently oriented MgO inclusions.

Keywords: Spinel, crystal chemistry, XRD, inclusion, periclase, electron backscatter diffraction

Introduction

Magnesium vanadate spinel, MgV_2O_4, has been the subject of extensive studies in earth and planetary science because the distribution of V is thought to be controlled primarily by spinel-like oxides during magmatic differentiation and evolution (cf. Canil 1999; Lee et al. 2003; Papike et al. 2004; Karner et al. 2006). Since V can occur in four valence states (V^{2+}, V^{3+}, V^{4+}, and V^{5+}) in nature, its redox system has been used as an oxybarometer for terrestrial or planetary interiors (cf. Sutton et al. 2005). Natural spinel may contain a significant amount of vanadium. For example, a suite of vanadian magnesiochromites, $Mg(Cr_{2-x}V_x)O_4$, found in the Sludynaka metamorphic complex in Russia contains a spinel with x = 0.95, nearly 50% of the octahedral site (Lavina et al. 2003a).

Structurally, vanadium spinel (AV_2O_4, where A = Mg, Zn, Cd, etc.) represents one of the most typical geometrically magnetic-frustrated systems, due to its unfilled *d*-orbitals and possible presence of different valence states. At low temperatures, a cubic-to-tetragonal phase transition, attributed possibly to the Jahn-Teller effect and spin ordering, has been observed in vanadium spinel, and the relationship between magnetic properties and its crystal structure has been discussed (Mamiya et al. 1997; Motome and Tsunetsugu 2005; Di Matteo et al. 2005).

The spinel unit cell (space group $Fd\bar{3}m$, no. 227) consists of a slightly distorted cubic close-packed array (CCP) of oxygen atoms with 1/8 of the tetrahedral sites (T) and 1/2 of the octahedral sites (M) occupied by various cations (Hill et al. 1979). A variety of cations can be accommodated in the T and M sites. There are two extreme cation distribution states: the normal spinel, $^{T}X^{M}(Y_2)O_4$, and the inverse one, $^{T}Y^{M}(XY)O_4$, where X and Y represent divalent and trivalent cations, respectively. Most natural spinels exhibit an intermediate configuration between these two states, $^{T}(X_{1-i}Y_i)^{M}(X_iY_{2-i})O_4$, where $0 \le i \le 1$. Many physical properties of spinel, such as magnetism, electrical conductivity, bulk modulus, thermal expansion, and compressibility, are largely influenced by the cation distribution (order-disorder) (Hazen and Yang 1999). Materials with the spinel structure are also radiation-resistant due to the ease of exchange between the two cation sites (cf. Bordes et al. 1995; Devanathan et al. 1996).

The presence of a small amount of cations in the interstitial sites of the spinel structure has been observed previously. For example, Fleet (1981) studied a natural, end-member magnetite with single-crystal X-ray diffraction and observed very weak but significant residual electron density on the difference Fourier maps at the interstitial tetrahedral site (8*b*). He suggested that

* E-mail: uchidah@email.arizona.edu

this electron density was likely to result from the presence of interstitial Fe^{3+} atoms coupled with corresponding vacancies at the M site.

Other examples of point defects in spinel and spinel-type structures include cation vacancies in natural magnetite (Menegazzo et al. 1997), maghemite, $Fe^{3+}(Fe^{3+}_{5/3}\square_{1/3})O_4$, (Somogyvári et al. 2002), synthetic ferrite, $(Mg_{0.22}Mn_{0.07}Fe_{0.71})_{3-\delta}O_4$, (Kang and Yoo 1999), $Al_{2/3}(Al_{2/3}V_{4/3})O_4$ (Reid and Sabine 1970), and in σ-alumina phase, $Al(Al_{5/3}\square_{1/3})O_4$, (Guse and Saalfeld 1990). In addition, oxygen deficiencies, oxygen excess at interstitial sites, and defect clustering in synthetic $LiMn_2O_4$ spinel have been described by Hosoya et al. (1997), Sugiyama et al. (1997), and Kanno et al. (1999). Many of the Cr-V bearing spinels from the Sludynaka metamorphic complex in Russia show extensive interstitial-vacancy point defects (Lavina et al. 2003b).

In this paper, we report an experimental study on a synthetic Mg-V spinel sample by means of a combination of X-ray diffraction (XRD), electron microprobe analysis (EMPA), and electron backscatter diffraction (EBSD) coupled with X-ray energy dispersive spectroscopy (XEDS). Our results show that the Mg-V spinel contains periclase (MgO) inclusions that have the same crystallographic orientation as the spinel matrix, which complicates the analysis of the X-ray diffraction intensities collected from the spinel crystal and could lead to a misinterpretation of structural details.

Experimental methods

Sample synthesis

Magnesium vanadate spinel was synthesized at 1 bar and 1200 °C at an oxygen fugacity equivalent to 1.3 $\log f_{O_2}$ units above the fayalite-magnetite-quartz (FMQ) buffer, from a mixture of MgO and V_2O_3 (99.995% pure). The material was placed on a Re wire loop in the hot spot of a Deltech vertical furnace. Oxygen fugacity was controlled by mixing CO and CO_2 in a reference furnace at 1200 °C, where the desired emf was adjusted before the introduction of the sample. The sample was held in the hot spot for 72 h, and then quenched by rapid removal. The synthesis products are clear octahedra of periclase and black spinel crystals, ranging from 30 to 50 μm in size.

Microprobe analysis

Five spinel crystals were selected from the same synthesis run and analyzed on a Cameca SX50 electron microprobe, using an acceleration voltage of 15 kV, a beam current of 20 nA, beam diameter of 2 μm, and 20 s counting times. Natural diopside and pure metallic vanadium were used as standards. Approximately 10 points were analyzed on the inclusion-free regions of each crystal. The chemical formula of the spinel, $Mg_{1.37}V^{3+}_{1.26}V^{4+}_{0.37}O_4$, was determined based on the analyses of the five crystals (Table 1). The amount of VO_2 was estimated by adjusting the sum of cation numbers to three and the total cation charge of eight. The back-scattered electron (BSE) images showed the presence of Mg-rich inclusions in all of these spinel crystals (Figs. 1a and b). However, the inclusions were too small (≤3 μm) for an accurate chemical analysis. The crystals in Figures 1a and 1b were oriented and polished to parallel to (001) and (111) planes, respectively. The inclusions in these crystals appear to exhibit specific crystallographic orientations, with fourfold and threefold symmetry, respectively.

Table 1. Chemical composition of MgV_2O_4 spinel

Oxide	wt%
MgO	30.9(9)
V_2O_3	68.1(7)
Total	99.0(6)
Cations based on 4 oxygen atoms	
Mg	1.37(3)
V^{3+}	1.26(6)
V^{4+}	0.37(3)
Total	3.00

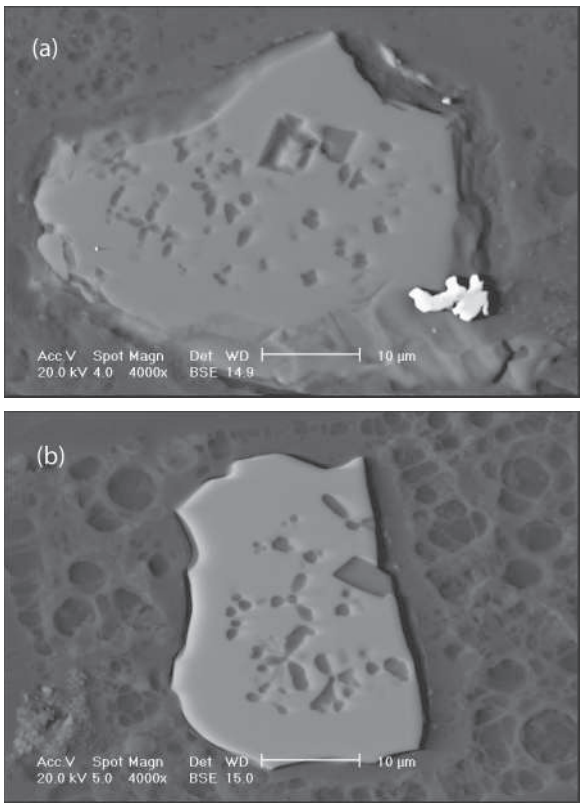

Figure 1. BSE images of (**a**) the selected crystal oriented and polished parallel to (001) planes, and (**b**) a crystal from the same synthesis oriented parallel to (111). The inclusions in these crystals appear to follow specific crystallographic orientations, with fourfold and threefold patterns, respectively.

EBSD/XEDS

The crystal was placed on a vibratory polisher with 0.05 μm colloidal silica suspension for approximately 10 m to obtain optimal diffraction patterns. An EDAX-TSL OIM 4.6 EBSD (electron backscatter diffraction) system coupled with an EDAX Genesis 4.5 XEDS system was employed to determine the chemistry of the Mg-rich inclusions and their crystallographic orientation with respect to the spinel phase. These systems were mounted on an FEI XL30 Scanning Electron Microscope (SEM). The XEDS spectra at 20, 15, 12, and 10 kV were measured to quantify the excitation volumes for the inclusion as a function of acceleration voltage. The calculated excitation volumes at those voltages are 8, 1, 0.4, 0.1 μm^3, respectively. The height of V peaks decreased at lower voltages, indicating that the presence of V at higher voltages is the result of interference with the matrix. Therefore, we conclude that the inclusions are pure MgO. For phase and orientation mapping, the sample was tilted approximately 75° and analyzed with an acceleration voltage of 20 kV. To map out the orientation relationships in the crystal, EBSD patterns were systematically collected and automatically indexed to obtain individual crystallographic orientations over an array of measurement points. Since the crystal structures of the matrix and inclusions are quite similar, it is difficult to reliably differentiate the two phases from each other based on EBSD patterns alone. Thus, XEDS counts for Mg, V, and O were simultaneously collected at each measurement point as well (Nowell and Wright 2004). The phases were differentiated based on Mg content. The phase differentiation results are shown as a map in Figure 2a where the phases are represented by different colors (online only); the spinel is represented in red and the MgO phase in green. Figure 2b shows an orientation map where the points are colored according to the crystallographic plane vector that is perpendicular to the polished sample. The pink color indicates that the spinel as well as most of the inclusions have the same orientation, approximately (001) planes parallel to the polished surface. One exceptional grain at the top right corner exhibits (101) planes parallel to the polished surface. Diffraction patterns

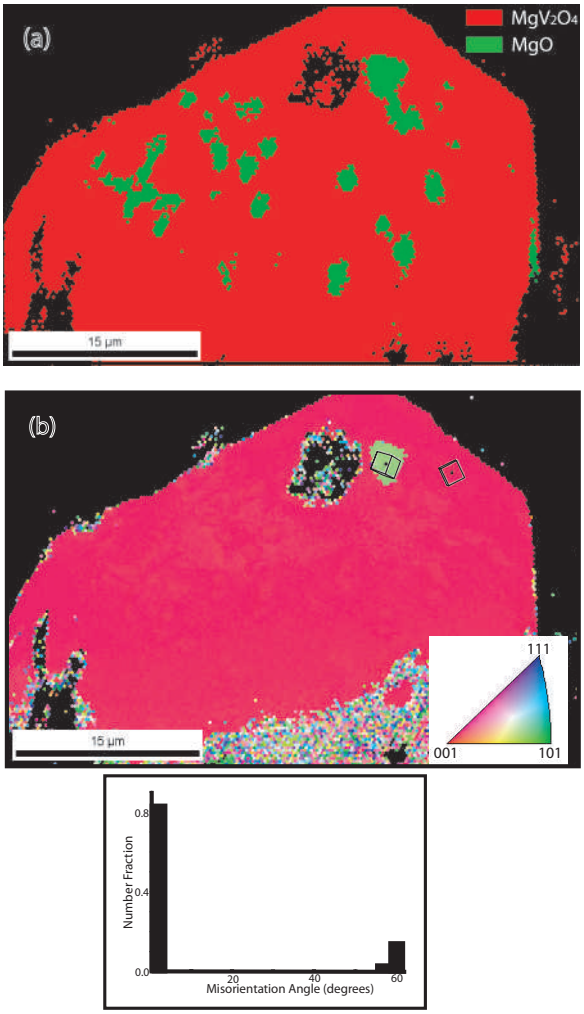

FIGURE 2. XEDS maps and statistics. (**a**) Phase map with the periclase phase in green or light gray and the spinel phase in red or dark gray (undetermined in black) (**b**) Orientation map. Regions having the same crystallographic orientation are represented by the same color. Spinel matrix and most inclusions have the same crystallographic orientation (001) as indicated by reddish pink or dark gray. One inclusion is misoriented from the matrix and shown in light green or light gray indicating (101) orientation. The unit-cell symbols are also inserted to indicate the two different orientations observed in this crystal. The histogram on the bottom shows the normalized distribution of misorientation across the grain boundaries. This shows approximately 60° misorientation between the spinel matrix and the grain in green. Note that the random colored points at the edges of the crystal are misindexed points for which poor quality patterns were obtained, thus these were excluded from the analysis. (See online version for color.)

of spinel matrix and the inclusions are shown in Figures 3a and 3b, respectively, which also confirm their orientation.

Single-crystal X-ray diffraction

A spinel fragment of 30 × 40 × 50 µm (Fig. 1a) was selected based on the sharpness of X-ray diffraction peaks. X-ray data were collected on a Bruker X8 APEX single-crystal diffractometer, using Mo$K\alpha$ radiation and a graphite monochromator, equipped with a 4K × 4K CCD area detector. Intensities were corrected for Lorentz and polarization factors, and absorption correction was performed using SADABS (Sheldrick 2005). No systematic absence violations or inconsistent

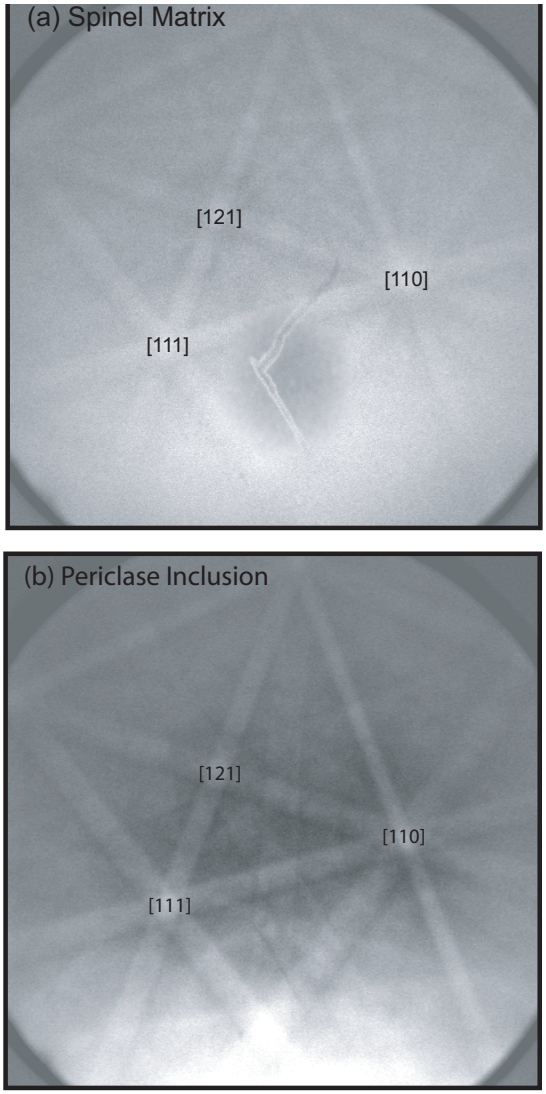

FIGURE 3. EBSD patterns of (**a**) spinel matrix and (**b**) periclase inclusion. Kikuchi lines demonstrate that the two phases have the same crystallographic orientation.

TABLE 2. Summary of crystal data and X-ray data

Chemical formula*	$Mg_{1.37}(V^{3+}_{1.26}V^{4+}_{0.37})O_4$
Chemical formula weight	116.28
Crystal size (mm)	0.03 × 0.04 × 0.05
Synthesis conditions	1200 °C, 1 bar, FMQ + 1.3
Space group	$Fd\bar{3}m$ (No. 227)
a (Å)	8.4170(7)
V (Å^3)	596.31(9)
Z	8
ρ_{calc} (g/cm^3)	4.049
λ (Å)	0.71073
μ (mm^{-1})	5.44
θ range for data collection	4.19–57.05
Collected reflections	1705
Unique reflections	228
Unique reflections with $I > 2\sigma(I)$	210
R(int)	0.017

* Chemical formula calculated from microprobe analysis based on four oxygen atoms.

equivalents were observed. The summary of the crystal and X-ray data is given in Table 2. The structure was refined with SHELXL-97 (Sheldrick 1997) using ionic scattering curves for Mg^{2+}, V^{3+}, and O^{2-} from Doyle and Turner (1968). The refined parameters include scale factor, secondary extinction coefficient, oxygen coordinate, and anisotropic displacement parameters. When constrained to ideal MgV_2O_4 stoichiometry, the refinement yielded a significantly higher *R* factor compared to the one with both T and M site occupancies allowed to vary. Therefore, several refinements were carried out to determine the site occupancies of the T and M sites (see below).

The preliminary refinement was performed with an assumption that the specimen was a single spinel phase. This resulted in residual electron density (4.46 $e^-/Å^3$) on the difference Fourier maps at one of the supposedly unoccupied octahedral sites (16*c*), M'. When Mg (0.052 apfu) was assigned to this site, the residual electron density decreased to 0.51 $e^-/Å^3$ and the R_1 and wR_2 decreased from 0.032 and 0.068 to 0.020 and 0.042, respectively. Furthermore, the refinement suggested the presence of a minor amount of vacancy, ~0.035 apfu in the T site, and additional Mg or vacancy in the M site. Since our synthesis products contain periclase inclusions, we constrained the M site occupancy to be V + Mg =1.0 and obtained a structural formula, $^{T}(Mg_{0.966}\square_{0.034})^{M}(V^{3+}_{1.422}V^{4+}_{0.218}Mg_{0.360})^{M'}Mg_{0.105}O_4$, where the amount of V^{4+} was introduced for charge balance.

Considering the close relationship between the spinel and the periclase structures and the fact that the *a* dimension of the investigated spinel (8.4170 Å) is almost twice that of MgO (4.2128 × 2 = 8.4256 Å; Zhang 2000), the periclase reflections can be superimposed onto the spinel ones. To explore this possibility, we adjusted our intensity data by subtracting estimated contributions from the periclase reflections from our original data. Iterative structural refinements were performed using modified intensity data sets with varying MgO volumes. The lowest *R* factors (R_1 = 0.021and wR_2 = 0.045) were achieved when the MgO volume was 9% of the total, resulting in a maximum electron residue of 0.67 $e^-/Å^3$ and no vacancy in the T site. Consequently, we assumed full occupancy for the T site. The final structural formula is $^{T}Mg^{M}(V^{3+}_{1.368}V^{4+}_{0.316}Mg_{0.316})O_4$.

DISCUSSION

Spinel-periclase crystal structural relationship

Point defects, including interstitial cations and vacancies in rock salt structures (*Fm*3*m*) such as wüstite, $Fe_{1-x}O$, and periclase, MgO, have been examined extensively (cf. Roth 1960; Hazen and Jeanloz 1984; Gibson et al. 1994; Karki and Khanduja 2006). The phase with intermediate composition, (Mg, Fe)O, is thought to be a major mantle component and its structural properties associated with point defects at high pressure is of great importance for understanding mantle rheology (Jeanloz and Hazen 1993). Wüstite is always observed to be nonstoichiometric, and charge balance can be obtained by introducing Fe^{3+} in small spinel domains. The

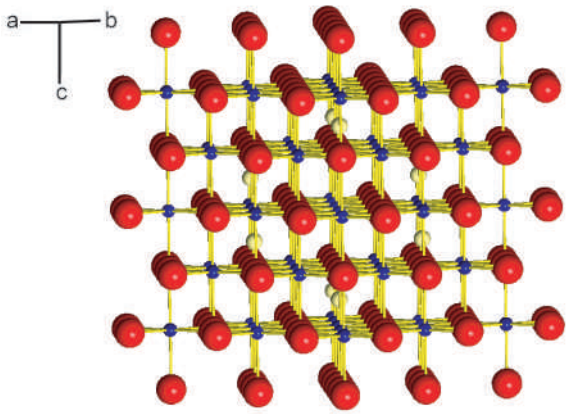

FIGURE 4. Doubled rock-salt unit cell with interstitial atoms (light-colored spheres) at the tetrahedral site. Oxygen atoms are represented by large spheres and the octahedral site by small dark spheres. (Color online.)

structural relationship of wüstite with spinel as its superlattice was discussed by Roth (1960). Both structures exhibit cubic symmetry with spinel cell dimensions roughly double those of wüstite. Oxygen atoms in both structures are cubic close packed. With the distorted oxygen packing of spinel, there are 2 sets of octahedral sites (16*c* and 16*d*) and 2 sets of tetrahedral sites (8*a* and 8*b*). If the oxygen packing is ideal or undistorted and both octahedral sites are occupied, then the structure becomes topologically equivalent to rock salt. When one of the tetrahedral sites is occupied, the nearest octahedral site is likely to be vacant due to electrostatic repulsion between cations. Figure 4 shows the doubled rock salt unit cell with interstitial atoms (light-colored) in the T site. Roth (1960) observed the presence of Fe atoms in the interstitial T site and vacancies in the M site in wüstite, $Fe_{0.940}O$ and $Fe_{0.926}O$, through neutron diffraction studies. He discussed the coalescence of point defects, resulting in regions of a "magnetite-like" cluster as well as regions of single interstitial atoms. The structure and arrangement of such defect clusters were also studied, for example, by Catlow and Fender (1975) and Andersson and Sletnes (1977). Welberry and Christy (1995, 1997) examined diffuse X-ray diffraction patterns from wüstite, which arise from the presence of defect clusters forming a highly disordered, inhomogeneous structure, to investigate the defect distribution, defect cluster size, and lattice strain.

Based on the previous observations, we initially modeled the structure of our sample with the interstitial octahedral sites partially occupied by Mg atoms and the neighboring tetrahedral sites with vacancies due to the short tetrahedral-octahedral distance (T–M' = 1.822 Å) as illustrated in Figure 5a. However, the presence of coherently oriented periclase inclusions, as observed in our sample, could produce the same X-ray diffraction patterns with residual electron density at the M' site. Therefore, we considered a second model in which periclase inclusions share the common oxygen layers with spinel matrix. Figure 5b illustrates the MgO structure coherent with the spinel structure, in which X-ray diffraction peaks of periclase necessarily coincide perfectly with those of spinel. The epitaxial relation between spinel and rock salt structures is well documented in the studies of microstructures and formation mechanism of spinel in other oxides. Wang and Shen (1998), Tsai et al. (2004), and Li and Shen (2004) examined, using analytical electron microscopy (AEM), spinel precipitates formed in oxides with the rock-salt structure: Al-doped $Ni_{1-x}O$, MgO–$Co_{1-x}O$, and Zr-doped $Co_{1-x}O$, respectively. Upon sintering and annealing, they found that the defects would cluster in their oxides to form paracrystals with the spinel-type lattice, e.g., $Co_{3-\delta}O_4$, which could further order to spinel. The formation of spinel precipitate depends on the relative charge and size of the elements in the reaction (Tsai et al. 2004). Given the similarities between the rock salt and spinel structures, inclusions of compounds with rock salt structure could be common in spinel (Pyatikop 1971), especially when the chemistry constrains cell edges of the rock salt component to half those of the spinel component.

Comparison of refinement results between two models: Structural effect of MgO inclusions

In many cases, correct crystallographic models can be discriminated from incorrect ones by comparing disagreement

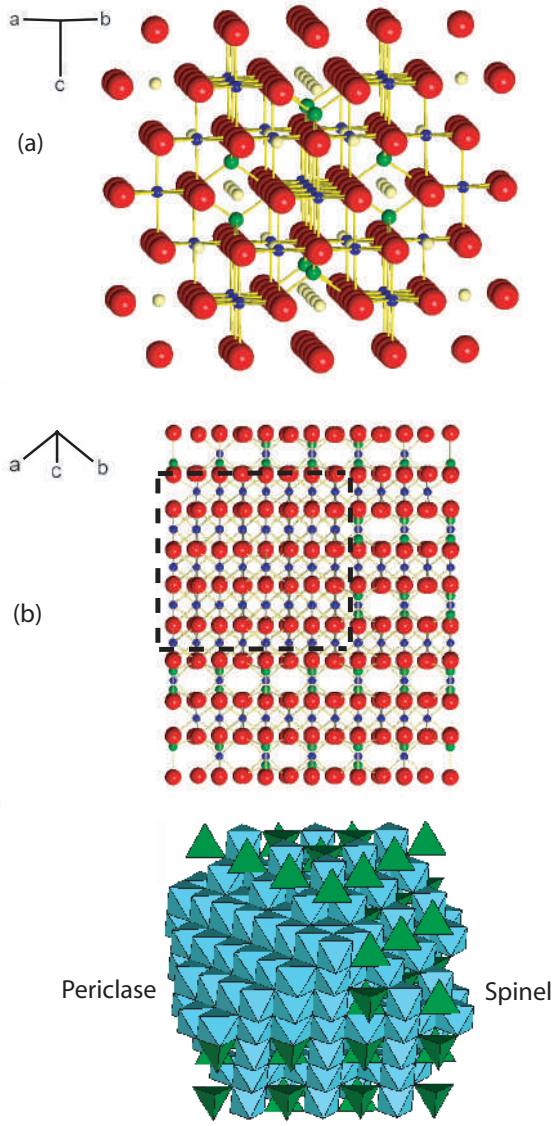

FIGURE 5. Two possible structural interpretations of our X-ray diffraction data. Oxygen atoms are represented by large spheres. (**a**) Model A: the spinel structure showing the tetrahedral site, T (green or gray spheres), the octahedral site, M (small dark spheres), and the interstitial octahedral site, M' (small light-colored spheres). When the M' site is occupied, the T site is likely to be vacant due to electrostatic repulsion (T-M' = 1.822 Å). Each sphere at the M' site represents 0.053 Mg occupancy. (**b**) Model B: a periclase domain (marked with the dotted box) embedded in the spinel matrix, viewed down on $[\bar{1}12]$ (above), and on $[\bar{1}\bar{1}1]$ (below). In the figure above, the tetrahedral site is represented by green or gray spheres and the octahedral site by small dark spheres. Note that the oxygen atoms and the M' sites are continuous. (Color is online.)

factors (GOF, R_1, and wR_2) and/or atomic displacement parameters. However, in our sample, a comparison of two models (A: a single spinel phase with interstitial Mg atoms; B: a spinel phase with MgO contribution subtracted) in Table 3 shows that they have similar disagreement factors and the same displacement parameters within 1σ. Nevertheless slight differences (3σ) in the bond distances and the oxygen coordinate (*u*) allow us to compare these two models.

On the one hand, in model B, the observed octahedral bond distance (M-O) is 2.0224(5) Å, close to the optimized value, V^{3+} – O = 2.022(7) (Lavina et al. 2002), while the observed tetrahedra-oxygen bond distance (T-O) is 1.9704(8) Å, which agrees well with T-O, 1.971 Å, of synthetic MgV_2O_4 (Mamiya and Onoda 1995). Note that this value for ^{T}Mg-O is larger than the optimized value, 1.966 Å (Lavina et al. 2002). As discussed by Lavina et al. (2003a), this lengthening of T-O is caused by "dragging effect" of certain cations in the M site (V in this case), responsible for change in T-O, which maintains distortion of oxygen packing (*u*) and provides the shielding between high-charged cations.

On the other hand, in model A, M-O = 2.0249(5) is longer and T-O = 1.9657(8) is shorter than those in model B. In addition, the *u* parameter in model A, 0.25984(6), lies between the value for ideal CCP, 0.25, and the value in model B, 0.26015(6), indicating the decrease in CCP distortion with the presence of M'. These observed values are consistent with a model of spinel with randomly distributed interstitial cations at M': modification of oxygen packing, indicated by *u*, and the T-O shortening due to interstitial V at the M' site, as observed in natural V-Cr bearing defect spinels (Lavina et al. 2003b). The same result can be obtained by averaging the ideally cubic close-packed structure (M-O = 2.1042 Å and T-O = 1.8223 Å for *u* = 0.25 and *a* = 8.4170 Å) and distorted close-packed structure, as shown in this study.

Analysis of site occupancy and unit-cell length

While the refinement for model B indicated full Mg occupancy at the T site, it also indicated that the M site has lower scattering power than for full V occupancy. In the literature, occurrence of vacancies has been mostly reported at the M site in spinel and spinel-type structure (Menegazzo et al. 1997; Guse and Saalfeld 1990; Somogyvári et al. 2002; Lavina et al. 2005). To determine whether the M site contains Mg or vacancy (□) in our sample, we performed two refinements: (1) V + Mg and (2) V + □ for the M site occupancy, and then we compared the observed T-O, M-O, *a*, and *u* with the calculated ones using the bond distances for spinel in Lavina et al. (2002, 2003a): ^{T}Mg-O = 1.971 Å, ^{M}Mg-O = 2.082 Å, $^{M}V^{3+}$-O = 2.022 Å, and ^{M}□-O = 2.11 Å. For $^{M}V^{4+}$-O, the value 1.96 Å was used based on the values 1.38 Å for O and 0.58 Å for V^{4+} given by Shannon (1976). The values for *a* and *u* were calculated using the following equations, with M-O being weighted according to the distribution of Mg, V, and vacancies at the M site:

$$a = \frac{8}{11\sqrt{3}}\left[5(\text{T-O}) + \sqrt{33(\text{M-O})^2 - 8(\text{T-O})^2}\right]$$

and

$$u = \frac{0.75R - 2 + \sqrt{(33/16)R - 0.5}}{6(R-1)},$$

respectively, where $R = (\text{M-O})^2/(\text{T-O})^2$. The calculated and refined parameters show a significantly better match when (V + Mg) is assumed to occupy the M site than when (V + □) is assumed,

TABLE 3. Comparison of refinement results for the two models

	Model A	Model B
No. of parameters refined	10	8
Goodness-of-fit	1.135	1.181
R factors [$I > 2\sigma(I)$]	R_1= 0.017, wR_2=0.042	R_1= 0.018, wR_2=0.045
R factors (all)	R_1= 0.020, wR_2=0.042	R_1= 0.021, wR_2=0.045
u	0.25984(6)	0.26015(6)
U_{11}(T)	0.00629(16)	0.00615(14)
U_{11}(M)	0.00560(6)	0.00561(6)
U_{12}(M)	–0.00019(3)	–0.00020(3)
U_{11}(O)	0.00774(14)	0.00749(13)
U_{12}(O)	–0.00064(9)	–0.00088(9)
T-O	1.9657(8)	1.9704(8)
M-O	2.0249(5)	2.0224(5)
M′-O	2.1902(5)	–
V(T)	3.8985	3.9254
V(M)	10.9592	10.9133
V(M′)	13.8870	–
site occ (T)	0.966(8) Mg	1.00 Mg
site occ (M)	0.820(10) V + 0.180 Mg	0.842(7) V + 0.158 Mg
site occ (M′)	0.053(3) Mg	–

Notes: In model A, the interstitial Mg atoms are disseminated through the crystal. In model B (preferred), periclase and spinel have distinct domains, but share continuous oxygen layers. The periclase contribution was subtracted from the total intensity for the refinement.
Tetrahedral site (T) located at [1/8, 1/8, 1/8] (8*a*), $U_{11} = U_{22} = {}_{33}$, $U_{12} = U_{13} = U_{23} \equiv 0$.
Octahedral site (M) located at [1/2, 1/2, 1/2] (16*d*), $U_{11} = U_{22} = U_{33}$, $U_{12} = U_{13} = U_{23}$.
Octahedral site (M′) located at [0, 0, 0] (16*c*), $U_{11} = U_{22} = U_{33}$, $U_{12} = U_{13} = U_{23}$.
Oxygen (O) located at [*u*, *u*, *u*] (32*e*), $U_{11} = U_{22} = U_{33}$, $U_{12} = U_{13} = U_{23}$.
The anisotropic displacement parameters for the M′ site are constrained to be those of the M site.

TABLE 4. Refinement results for model B with the octahedral site occupied by (1) V + Mg (preferred) and (2) V + □

	(1) V + Mg			(2) V + □		
	obs	calc	Δ	obs	calc	Δ
T-O (Å)	1.9704(8)	1.971	~0.001	1.9701(8)	1.971	~0.001
M-O (Å)	2.0224(5)	2.0217	0.0007	2.0225(5)	2.0148	0.0077
a (Å)	8.4170(7)	8.4160	0.0010	8.4170(7)	8.3971	0.0199
u	0.26015(6)	0.26021	0.00006	0.26014(5)	0.26052	0.00038
V^{3+} (apfu)	0.684(7)			0.708(3)		
V^{4+} (apfu)*	0.158			0.219		
Mg (apfu)	0.158			–		
□	–			0.073		
Mg/V	0.78			0.54		

Notes: The tetrahedral site was constrained to be fully occupied by Mg. The observed T-O, M-O, *a*, and *u* are compared with the calculated ones (see text).
* Calculated based on charge balance. Mg/V from microprobe analysis: 0.84.

as summarized in Table 4. The magnesium-to-vanadium ratio obtained from the microprobe analysis (0.84) also matches better with the former refinement (0.78) (Table 4). The substitution $4/3V^{3+} \leftrightarrow V^{4+} + 1/3\square$ at the M site causes significant decrease in the calculated unit-cell length, whereas the substitution $2V^{3+} \leftrightarrow Mg + V^{4+}$ decreases it very slightly, and therefore, the observed unit-cell length matches well with that calculated for the refined formula.

The unit-cell length of the investigated spinel crystal is 8.4170(7) Å. In our sample, the MgO phase probably has not significantly affected the averaged unit-cell length because of its low abundance and the fact that the unit-cell length of MgO (*a* = 4.2128 Å; Zhang 2000) is approximately half of the MgV_2O_4 spinel. This conclusion may be additionally supported by the absence of streaks or splits in our diffraction peaks, which indicates much less lattice strain between the phases, MgO and MgV_2O_4, than the ones between spinel precipitates and their corresponding oxides reported in the literature (cf. Tsai et al. 2004).

Role of X-ray diffraction in analysis of spinel and rock salt mixtures

We presented two possible structural interpretations of the investigated spinel crystal based on the observed residual electron density from the difference Fourier maps. Confirmation that the periclase lattice is oriented in the same way as spinel enabled us to eliminate the model in which the interstitial Mg was distributed through the spinel structure. Instead, we found that the electron residue is a consequence of the periclase inclusions which coherently share the oxygen atoms and the octahedral cations of the spinel structure. We were able to separate the periclase contribution in our X-ray intensity data, and obtained the structural formula for the spinel phase, $^{T}Mg^{M}(V^{3+}_{1.368}V^{4+}_{0.316}Mg_{0.316})O_4$ with the T site fully occupied. This agrees well with the chemical formula obtained from the microprobe analysis.

X-ray diffraction alone cannot discriminate which model is more appropriate for a physical interpretation of our sample because the two models generate similar disagreement factors and displacement parameters, and consistent bond distances as well as oxygen coordinate corresponding to their refined models. These two structural interpretations of the diffraction data are significantly different from the view point of chemical and physical properties of the crystal.

It is possible for MgV_2O_4 spinel to display an intermediate stage between point defects disseminated throughout the crystal and distinct domains. While different crystals may exhibit different degrees of dissemination of the (M' + □), this study showed conclusively that our sample had distinct domains of periclase in spinel.

ACKNOWLEDGMENTS

Funding for this study was provided by the Galileo Circle Scholarship and Tucson Gem and Mineral Society Scholarship to H. Uchida and by the NASA RTOP to K. Righter. We thank C.T. Prewitt and V.A. Valencia for their thoughtful suggestions and comments. We also thank K. Domanik for his assistance during microprobe analyses, and R.X. Fischer and S. Lucchesi for their careful reviews and comments.

REFERENCES CITED

Andersson, B. and Sletnes, J.O. (1977) Decomposition and ordering in $Fe_{1-x}O$. Acta Crystallographica A, 33, 268–276.
Bordes, N., Wang, L.M., Ewing, R.C., and Sickafus, K.E. (1995) Ion-beam induced disordering and onset of amorphization in spinel by defect accumulation. Journal of Materials Research, 10, 981–985.
Canil, D. (1999) Vanadium partitioning between orthopyroxene, spinel and silicate melt and the redox states of mantle source regions for primary magmas. Geochimica et Cosmochimica Acta, 63, 557–572.
Catlow, C.R.A. and Fender, B.E.F. (1975) Calculations of defect clustering in $Fe_{1-x}O$. Journal of Physics C: Solid State Physics, 8, 3267–3279.
Devanathan, R., Yu, N., Sickafus, K.E., and Nastasi, M. (1996) Structure and mechanical properties of irradiated magnesium aluminate spinel. Journal of Nuclear Materials, 232, 59–64.
Di Matteo, S., Jackeli, G., and Perkins, N.B. (2005) Orbital order in vanadium spinels. Physical Review B, 72, 020408.
Doyle, P.A. and Turner, P.S. (1968) Relativistic Hartree-Fock X-ray and electron scattering factors. Acta Crystallographica A, 24, 390–397.
Fleet, M.E. (1981) The structure of magnetite. Acta Crystallographica B, 37, 917–920.
Gibson, A., Haydock, R., and LaFemina, J.P. (1994) Stability of vacancy defects in MgO: The role of charge neutrality. Physical Review B, 50, 2582–2592.
Guse, W. and Saalfeld, H. (1990) X-ray characterization and structure refinement of a new cubic alumina phase (σ–Al_2O_3) with spinel-type structure. Neues Jahrbuch für Mineralogie—Monatshefte, 217–226.
Hazen, R.M. and Jeanloz, R. (1984) Wüstite ($Fe_{1-x}O$): A review of its defect

structure and physical properties. Reviews of Geophysics and Space Physics, 22, 37–46.
Hazen, R.M. and Yang, H. (1999) Effects of cation substitution and order-disorder on *P-V-T* equations of state of cubic spinels. American Mineralogist, 84, 1956–1960.
Hill, R.J., Craig, J.R., and Gibbs, G.V. (1979) Systematics of the spinel structure type. Physics and Chemistry of Minerals, 4, 317–339.
Hosoya, M., Ikuta, H., Uchida, T., and Wakihara, M. (1997) The defect structure model in nonstoichiometric $LiMn_2O_{4-\delta}$. Journal of the Electrochemical Society, 144, L52–L53.
Jeanloz, R. and Hazen, R.M. (1993) Composition limits of Fe_xO and the Earth's lower mantle. Science, 261, 923–924.
Kang, S.-H. and Yoo, H.-I. (1999) Nonstoichiometry (δ) and high-temperature thermodynamic properties of $(Mg_{0.22}Mn_{0.07}Fe_{0.71})_{3-\delta}O_4$ ferrite spinel. Journal of Solid State Chemistry, 145, 276–282.
Kanno, R., Kondo, A., Yonemura, M., Gover, R., Kawamoto, Y., Tabuchi, M., Kamiyama, T., Izumi, F., Masquelier, C., and Rousse, G. (1999) The relationships between phases and structures of lithium manganese spinels. Journal of Power Sources, 81–82, 542–546.
Karki, B.B. and Khanduja, G. (2006) Vacancy defects in MgO at high pressure. American Mineralogist, 91, 511–516.
Karner, J.M., Sutton, S.R., Papike, J.J., Shearer, C.K., Jones, J.H., and Newville, M. (2006) Application of a new vanadium valence oxybarometer to basaltic glasses from the Earth, Moon, and Mars. American Mineralogist, 91, 270–277.
Lavina, B., Salviulo, G., and Della Giusta, A. (2002) Cation distribution and structure modelling of spinel solid solutions. Physics and Chemistry of Minerals, 29, 10–18.
Lavina, B., Reznitskii, L.Z., and Bosi, F. (2003a) Crystal chemistry of some Mg, Cr, V normal spinels from Sludyanka (Lake Baikal, Russia): the influence of V^{3+} on structural stability. Physics and Chemistry of Minerals, 30, 599–605.
Lavina, B., Reznitskii, L.Z., and Della Giusta, A. (2003b) A new Mg-Cr-V oxide mineral from Sludyanka (SW Lake Baikal, Russia) with a spinel-like defect structure. Joint Congress AIC-SILS, 50.
Lavina, B., Princivalle, F., and Della Giusta, A. (2005) Controlled time-temperature oxidation reaction in a synthetic Mg-hercynite. Physics and Chemistry of Minerals, 32, 83–88.
Lee, C.-T.A., Brandon, A.D., and Norman, M. (2003) Vanadium in peridotites as a proxy for paleo-f_{O_2} during partial melting: Prospects, limitations, and implications. Geochimica et Cosmochimica Acta, 67, 3045–3064.
Li, M.-Y. and Shen, P. (2004) On the nucleation and paracrystal interspacing of Zr-doped $Co_{3-\delta}O_4$. Materials Science and Engineering B, 111, 82–89.
Mamiya, H. and Onoda, M. (1995) Electronic states of vanadium spinels MgV_2O_4 and ZnV_2O_4. Solid State Communications, 95, 217–221.
Mamiya, H., Onoda, M., Furubayashi, T., Tang, J., and Nakatani, I. (1997) Structural and magnetic studies on vanadium spinel MgV_2O_4. Journal of Applied Physics, 81, 5289–5291.
Menegazzo, G., Carbonin, S., and Della Giusta, A. (1997) Cation and vacancy distribution in an artificially oxidized natural spinel. Mineralogical Magazine, 61, 411–421.
Motome, Y. and Tsunetsugu, H. (2005) Orbital ordering and one-dimensional magnetic correlation in vanadium spinel oxides AV_2O_4 (A = Zn, Mg, or Cd). Physica B, 359–361, 1222–1224.
Nowell, M.M. and Wright, S.I. (2004) Phase differentiation via combined EBSD and XEDS. Journal of Microscopy, 213, 296–305.
Papike, J.J., Karner, J.M., and Shearer, C.K. (2004) Comparative planetary mineralogy: V/(Cr + Al) systematics in chromite as an indicator of relative oxygen fugacity. American Mineralogist, 89, 1557–1560.
Pyatikop, P.D. (1971) Microstructure and mineral composition of magnesium-aluminum spinel specimens synthesized under conditions of periclase excess and addition of chromite ore. Konstitutsiya i Svoystva Mineralov, 5, 115–118.
Reid, A.F. and Sabine, T.M. (1970) $AlVO_3$, a metal-deficient spinel. Journal of Solid State Chemistry, 2, 203–208.
Roth, W.L. (1960) Defects in the crystal and magnetic structures of ferrous oxide. Acta Crystallographica, 13, 140–149.
Shannon, R.D. (1976) Revised effective ionic radii and systematic studies of interatomic distances in halides and chalcogenides. Acta Crystallographica A, 32, 751–767.
Sheldrick, G.M. (1997) SHELX97 and SHELXS97. University of Göttingen, Germany.
——— (2005) SADABS v.2.10. University of Göttingen, Germany.
Somogyvári, Z., Sváb, E., Mészáros, G., Krezhov, K., Nedkov, I., Sajó, I., and Bourée, F. (2002) Vacancy ordering in nanosized maghemite from neutron and X-ray powder diffraction. Applied Physics A, 74, S1077–S1079.
Sugiyama, J., Atsumi, T., Hioki, T., Noda, S., and Kamegashira, N. (1997) Nonstoichiometry and defect structure of spinel $LiMn_2O_{4-\delta}$. Journal of Power Sources, 68, 641–645.
Sutton, S.R., Karner, J., Papike, J., Delaney, J.S., Shearer, C., Newville, M., Eng, P., Rivers, M., and Dyar, M.D. (2005) Vanadium K edge XANES of synthetic and natural basaltic glasses and application to microscale oxygen barometry. Geochimica et Cosmochimica Acta, 69, 2333–2348.
Tsai, T.M., Yang, K.C., and Shen P. (2004) Defect clusters and precipitation/oxidation of $MgO–Co_{1-x}O$ solid solution. Journal of Solid State Chemistry, 177, 3301–3309.
Wang, S.R. and Shen, P. (1998) On the spinel precipitation in Al-doped $Ni_{1-x}O$. Journal of Solid State Chemistry, 140, 38–45.
Welberry, T.R. and Christy, A.G. (1995) A paracrystalline description of defect distributions in wüstite, $Fe_{1-x}O$. Journal of Solid State Chemistry, 117, 398–406.
——— (1997) Defect distribution and the diffuse X-ray diffraction pattern of wüstite, $Fe_{1-x}O$. Physics and Chemistry of Minerals, 24, 24–38.
Zhang, J. (2000) Effect of pressure on the thermal expansion of MgO up to 8.2 GPa. Physics and Chemistry of Minerals, 27, 145–148.

MANUSCRIPT RECEIVED SEPTEMBER 8, 2006
MANUSCRIPT ACCEPTED MARCH 14, 2007
MANUSCRIPT HANDLED BY G. DIEGO GATTA